

## Theoretical Study of the Reaction of Atomic Hydrogen with Acetonitrile

Baoshan Wang,\* Hua Hou, and Yueshu Gu

School of Chemistry, Shandong University, Jinan 250100, P. R. China

Received: June 7, 2000; In Final Form: September 7, 2000

The reaction of atomic hydrogen with acetonitrile has been studied using the B3LYP and Gaussian-3 (G3) methods. The geometries and vibrational frequencies of various stationary points on the potential energy surface were calculated at the B3LYP level with the 6-311G(d,p) and 6-311++G(2d,2p) basis sets. The energetics were refined at the G3 level. The G3 barrier height has been calibrated using a test set including 39 well-established reactions. It is believed that the present potential energy surface is reliable within chemical accuracy. The title reaction starts in four manners, namely direct hydrogen abstraction, C-addition, N-addition, and substitution. The corresponding barrier heights (including ZPE corrections) are 12.0, 7.6, 9.6, and 44.7 kcal/mol, respectively. The kinetics of the reaction were studied using the TST and multichannel RRKM methodologies over the temperature range 300~3000 K, and were compared with the earlier experimental data. At lower temperatures, the C-addition step is the most feasible channel, and the major products are CH<sub>3</sub> and HCN at lower pressures. At higher temperatures, the direct hydrogen abstraction path leading to H<sub>2</sub> and CH<sub>2</sub>CN is apparently dominant.

### I. Introduction

Acetonitrile (CH<sub>3</sub>CN) is an important intermediate in a number of combustion processes.<sup>1</sup> The CH and CC bonds of CH<sub>3</sub>CN are very strong, due to their bond dissociation energies of 93.0 and 121.8 kcal/mol, respectively.<sup>2</sup> The isomerization reaction CH<sub>3</sub>CN → CH<sub>3</sub>NC involves an energy barrier of as high as 62.1 kcal/mol and is endothermic by 24 kcal/mol.<sup>3</sup> Therefore, the unimolecular reaction of CH<sub>3</sub>CN is of minor importance. It is conceivable that the bimolecular processes of CH<sub>3</sub>CN with the highly reactive radical species will be significant in flames. Meanwhile, the reactions of CH<sub>3</sub>CN are of interest in atmospheric chemistry.<sup>4</sup> This study is directed toward the determination of the energetics and kinetics of these reactions when the H atom is considered.

Although the reactions of CH<sub>3</sub>CN with F, Cl, O(<sup>3</sup>P), and OH have been fairly well investigated experimentally,<sup>4–6</sup> the reaction of CH<sub>3</sub>CN with atomic hydrogen—an important flame and atmospheric species—is rarely studied. Examination of the literature reveals only a single earlier study of this reaction.<sup>7</sup> In that work, the static products, i.e., HCN, CH<sub>4</sub>, and C<sub>2</sub>H<sub>6</sub>, were detected. The overall rate constant of production of HCN was determined to be  $k_{\text{HCN}} = 3.55 \times 10^{-12} \exp(-2927/T)$  cm<sup>3</sup> molecule<sup>-1</sup> s<sup>-1</sup> in the temperature range of 313~780 K and at the pressure of ~1 Torr. A chain characteristic propagated by the CN radical was supposed to interpret experimental findings. However, this assumption is questionable in view of the high endothermicity of channel 4:



The motivation of the current study is to characterize the H + CH<sub>3</sub>CN reaction on a sound theoretical basis. We carried out detailed ab initio molecular orbital (MO) and multichannel RRKM-TST calculations to elucidate the mechanism of the reaction and to calculate the rate constants for various channels at temperatures from 300 to 3000 K. The results are presented herein.

### II. Computation Procedure

Preliminary ab initio calculations using the UHF and UMP2 methods reveal that these unrestricted wave functions are significantly contaminated for the present open-shell doublet system. The expectation value of  $S^2$  is always around 1.0, which deviates from the correct value of 0.75 by up to 33%. It implies that these calculations cannot be reliable. Previous studies show that the density functional theory (DFT) is capable of annihilating spin contamination effectively.<sup>8</sup> Thus, a hybrid density functional B3LYP method, namely Becke's three-parameter nonlocal exchange functional<sup>9</sup> with the nonlocal correlation functional of Lee, Yang, and Parr,<sup>10</sup> was employed in this study. The potential energy surface (PES) was first examined at the B3LYP/6-311G(d,p) level. The geometries of all the reactants, products, intermediates, and transition states were fully optimized. Vibrational frequencies were obtained at the same level of theory for characterization of the nature of the stationary points. Subsequently, all the transition states were subject to intrinsic reaction coordinate (IRC)<sup>11</sup> calculations to confirm the connection between the designated reactants and products. Finally, the geometrical parameters of all stationary points were refined using the same method (B3LYP) but with a more flexible basis set, 6-311++G(2d,2p), and the vibrational frequencies were also recalculated at this level for zero-point energy (ZPE) corrections. At this higher level, the expectation values of  $S^2$  are always in the range 0.750~0.778 (see Table 1), implying the negligible spin contamination.

To obtain more reliable energies, the Gaussian-3 (G3) method,<sup>12</sup> which was used at the QCISD(T,full)/G3Large level, was utilized. In the current study, all essential single-point

\* Corresponding author.

TABLE 1: Relative Energies ( $\Delta E$ , ZPE-corrected, in kcal/mol) through the Reaction of H with CH<sub>3</sub>CN.

| species                             | $\langle S^2 \rangle^a$ | ZPE  | $\Delta E(\text{B3LYP})^b$ | $\Delta E(\text{G3})^c$ | $\Delta H_{298}^\circ{}^d$ | $\Delta H_{298}^\circ{}^{\text{expt.}}{}^e$ |
|-------------------------------------|-------------------------|------|----------------------------|-------------------------|----------------------------|---|
| H + CH <sub>3</sub> CN              | 0.750, 0.0              | 28.4 | 0.0                        | 0.0                     |                            |   |
| H <sub>2</sub> + CH <sub>2</sub> CN | 0.0, 0.767              | 25.8 | -12.6                      | -7.8                    | -13.1                      | -11.6 ± 0.2                                 |
| CH <sub>3</sub> + HCN               | 0.754, 0.0              | 28.9 | -6.7                       | -3.4                    | -4.9                       | -3.6 ± 1.3                                  |
| CH <sub>3</sub> + HNC               | 0.754, 0.0              | 28.3 | 7.0                        | 11.1                    | 9.9                        |   |
| H + CH <sub>2</sub> CNH             | 0.750, 0.0              | 27.4 | 22.3                       | 27.2                    | 27.2                       |   |
| CH <sub>4</sub> + CN                | 0.0, 0.758              | 31.1 | 18.4                       | 18.9                    | 17.2                       | 16.9 ± 0.8                                  |
| CH <sub>3</sub> CHN                 | 0.759                   | 34.3 | -25.0                      | -19.2                   | -22.3                      |   |
| <i>cis</i> -CH <sub>3</sub> CNH     | 0.755                   | 34.0 | -15.5                      | -8.7                    | -11.7                      |   |
| <i>trans</i> -CH <sub>3</sub> CNH   | 0.753                   | 34.5 | -19.8                      | -13.2                   | -16.2                      |   |
| CH <sub>2</sub> CHNH                | 0.778                   | 34.6 | -22.8                      | -15.8                   | -19.2                      |   |
| CH <sub>2</sub> CNH <sub>2</sub>    | 0.755                   | 34.5 | -5.8                       | -1.4                    | -1.5                       |   |
| TS1                                 | 0.760                   | 26.7 | 5.2                        | 12.0                    |                            |   |
| TS2                                 | 0.762                   | 29.4 | 5.2                        | 7.6                     |                            |   |
| TS3                                 | 0.767                   | 30.8 | 1.7                        | 6.5                     |                            |   |
| TS4                                 | 0.759                   | 28.9 | 4.9                        | 9.6                     |                            |   |
| TS5                                 | 0.753                   | 33.0 | -4.3                       | 3.0                     |                            |   |
| TS6                                 | 0.761                   | 30.0 | 13.1                       | 19.4                    |                            |   |
| TS7                                 | 0.761                   | 29.9 | 13.5                       | 19.9                    |                            |   |
| TS8                                 | 0.757                   | 31.0 | 18.1                       | 23.3                    |                            |   |
| TS9                                 | 0.763                   | 31.2 | 21.4                       | 27.0                    |                            |   |
| TS10                                | 0.757                   | 31.0 | 30.6                       | 39.9                    |                            |   |
| TS11                                | 0.756                   | 30.1 | 49.6                       | 57.8                    |                            |   |
| TS12                                | 0.761                   | 31.0 | 36.3                       | 43.6                    |                            |   |
| TS13                                | 0.768                   | 28.4 | 26.1                       | 33.4                    |                            |   |
| TS14                                | 0.758                   | 28.5 | 25.8                       | 34.8                    |                            |   |
| TS15                                | 0.764                   | 29.2 | 39.4                       | 44.7                    |                            |   |

<sup>a</sup> The average value of  $S^2$  before spin projection. <sup>b</sup> At the B3LYP/6-311++G(2d,2p) + ZPE level. The total energy of H + CH<sub>3</sub>CN is -133.25755 hartree. <sup>c</sup> At the G3 level. The total energy of H + CH<sub>3</sub>CN is -133.10743 hartree. <sup>d</sup> The calculated heats of reaction at 298.15 K at the G3 level. <sup>e</sup> Experimental enthalpies of formation at 298 K were taken from ref 16.

energies were calculated on the basis of the B3LYP/6-311++G(2d,2p) optimized geometries. Since the numbers of  $\alpha$  and  $\beta$  valence electrons do not change in the reaction, the empirical high-level correction in the G3 scheme was omitted. All of the molecular orbital calculations were performed using the GAUSSIAN 94 program.<sup>13</sup> Unless stated otherwise, the relative energies discussed below are the G3 energies, including the ZPE corrections.

### III. Results and Discussion

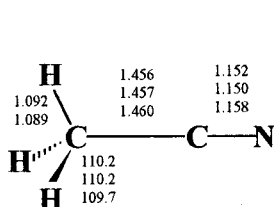
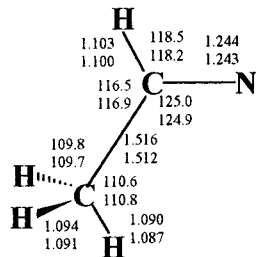
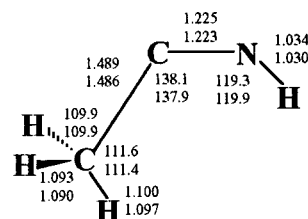
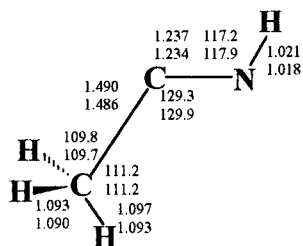
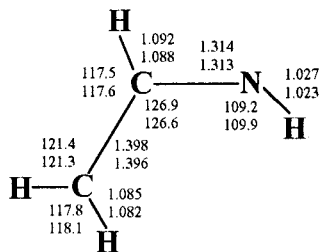
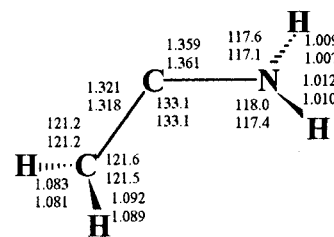
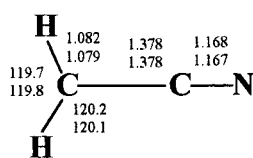
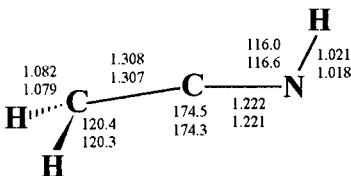
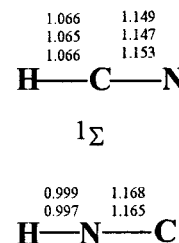
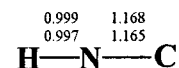
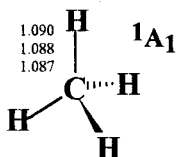
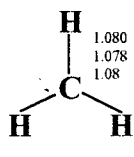
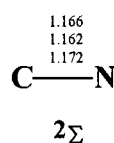
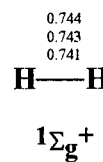
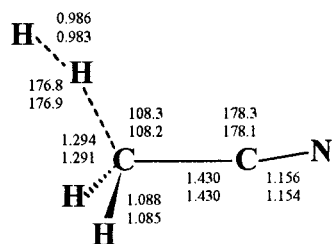
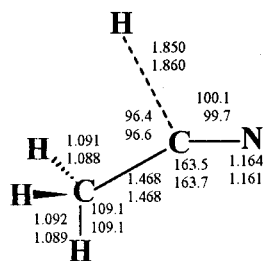
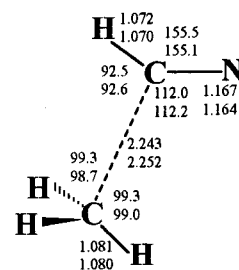
The geometries of the reactants, intermediates, products, and transition states are shown in Figure 1. The schematic potential energy profile of the title reaction is shown in Figure 2. The computed energetics by the B3LYP and G3 methods are listed in Table 1. The vibrational frequencies for various species are deposited as Supporting Information (Table S1).

**III.1 Reliability of the B3LYP and G3 Calculations.** Figure 1 shows that the geometries of various species obtained at the B3LYP/6-311G(d,p) level do not deviate significantly from those obtained at the B3LYP/6-311++G(2d,2p) level. For the reactant and product species, the theoretical bond lengths and angles agree very well with the experimental values.<sup>2</sup> Moreover, as shown in Table S1, the calculated vibrational frequencies are also in good agreement with the experimental measurements.<sup>14</sup> These comparisons reflect that the B3LYP/6-311++G(2d,2p) level might be apposite for both geometries and vibrational properties of the CH<sub>3</sub>CN system.

However, the B3LYP-DFT method has a known defect, e.g., the overestimation of the reacting X-H (C-H or N-H) bond lengths. This is always caused by the flatness of the potential energy surface. The looser structure at the B3LYP level will overestimate the preexponential factor because of the predicted larger inertial of moment. Fortunately, the error of such a drawback might not be serious (within a factor of at most 2) because: (i) the rate constant is determined mainly by the barrier height, (ii) the B3LYP frequencies are believed to be reliable,

and (iii) the Gaussian-n energy appears to be insensitive to the use of geometry under this condition. As a matter of fact, the B3LYP geometries have been shown to be successful in studying many reactions involving the reacting X-H bonds.<sup>15</sup> Certainly, the use of more sound levels of theory such as CCSD(T) to optimize geometries of the CH<sub>3</sub>CN system is very valuable and are reserved for future study.

It is believed that the G3 method performs well for thermochemistry.<sup>12</sup> As can be seen from Table 1, the reaction heats at 298.15 K for channels 1, 2, and 4 are in good agreement with the available experimental values.<sup>16</sup> However, since the G3 method was not designed specifically to determine transition state, is it reliable for transition state? As far as we know, there are few attempts made to determine this issue. Because in the current study the barrier height is most concerned, we take this opportunity to do such a calibration with respect to the accuracy of the G3-predicted barrier height. A total of 39 reactions whose barrier heights have been well established previously<sup>17-44</sup> were selected, as shown in Table 2. This test set covers abstraction, addition/elimination, and unimolecular reactions. It is worth noting that the well-studied H + HCN reaction,<sup>44</sup> which is analogous to the present H + CH<sub>3</sub>CN reaction, is also included. Those previous results refer to either the experimental measurements or the high-quality theoretical calculations. To make the conclusion more generalized, the conventional G3 scheme was used to calculate the barrier height (classical or ZPE-corrected) for each reaction. Evidently, the barrier heights at the G3 level are in reasonable agreement with the previous results for all 39 reactions. The average absolute deviation (AAD) is 1.12 kcal/mol, which is only slightly higher (by 0.11 kcal/mol) than that of the whole G2/97 test set at the G3 level. The maximum positive and negative deviations are +3.5 and -2.7 kcal/mol, respectively. In comparison with the latest results obtained at the multireference configuration interaction (MRCI) level with large correlation consistent basis set and at the CCSD(T)/6-311++G(3df,3pd)//6-311++G(d,p) level, the G3-calculated

**CH<sub>3</sub>CN, C<sub>3v</sub>, 1A<sub>1</sub>****CH<sub>3</sub>CHN, C<sub>s</sub>, 2A'****cis-CH<sub>3</sub>CNH, C<sub>s</sub>, 2A'****trans-CH<sub>3</sub>CNH, C<sub>s</sub>, 2A'****CH<sub>2</sub>CHNH, C<sub>s</sub>, 2A''****CH<sub>2</sub>CNH<sub>2</sub>, C<sub>1</sub>, 2A****CH<sub>2</sub>CN, C<sub>2v</sub>, 2B<sub>1</sub>****CH<sub>2</sub>CNH, C<sub>s</sub>, 1A'****1Σ****1Σ****1A<sub>1</sub>****2A<sub>2</sub>''****2Σ****1Σ<sub>g</sub><sup>+</sup>****TS1, C<sub>s</sub>, 2A'****TS2, C<sub>s</sub>, 2A'****TS3, C<sub>s</sub>, 2A'**

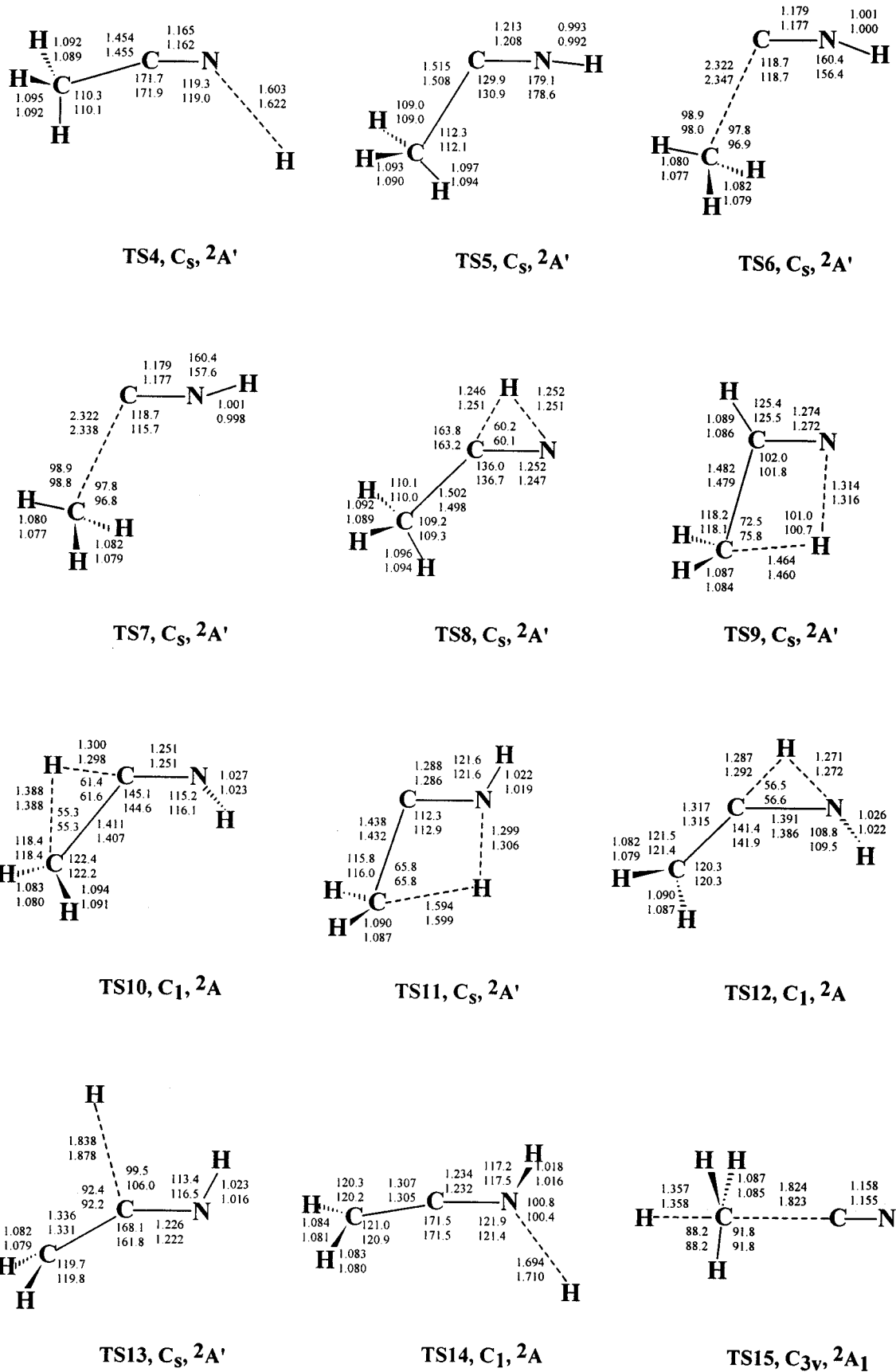


**Figure 1.** Optimized geometrical parameters for various species involved in the  $H + CH_3CN$  reaction. The first entry corresponds to the B3LYP/6-311G(d,p) value. The second entry corresponds to the B3LYP/6-311++G(2d,2p) value. The third entry corresponds to the experimental value. Bond distances are in angstroms. Bond angles are in degrees.

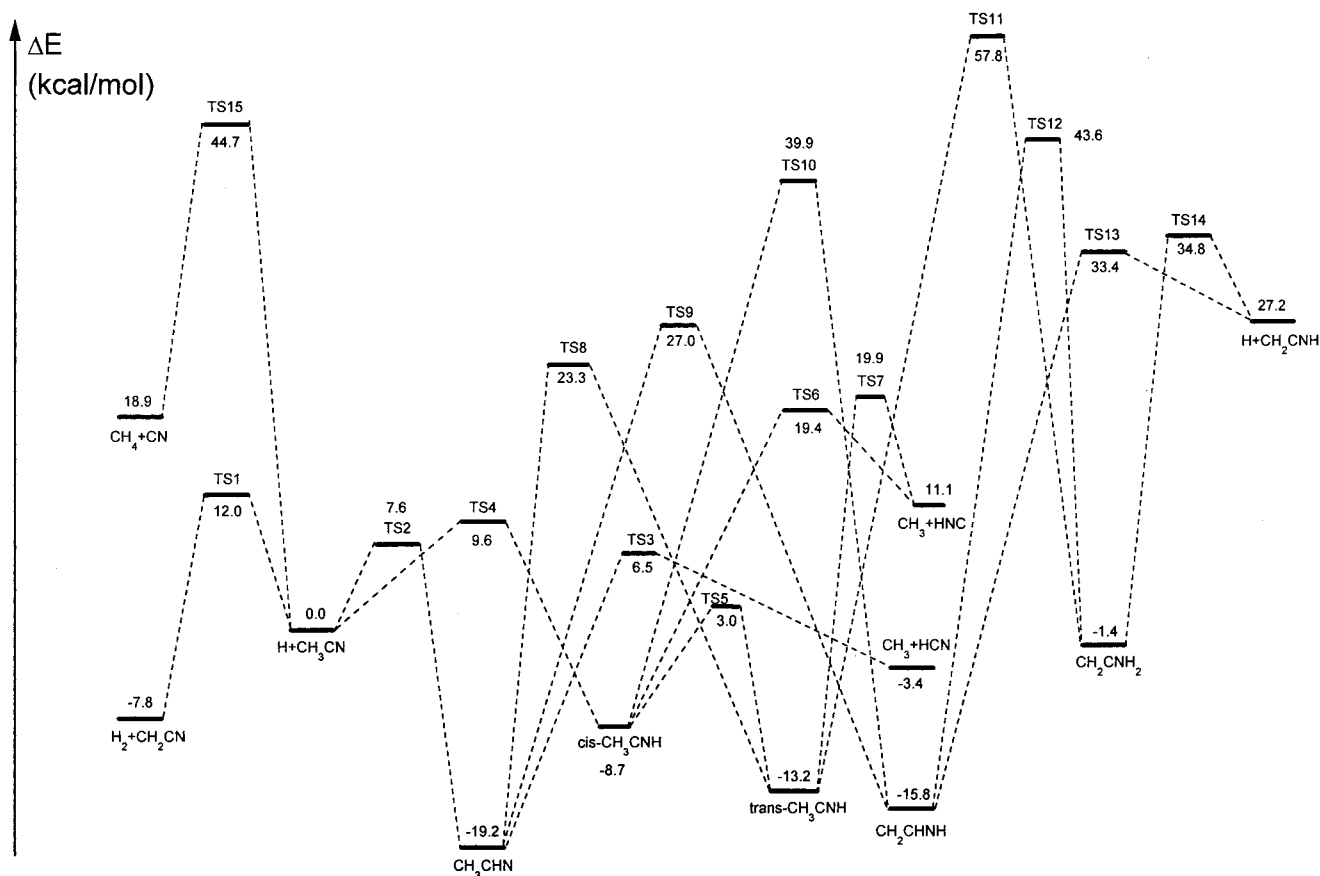


**Figure 2.** Energetic profile (in kcal/mol) of the potential energy surface for the H + CH<sub>3</sub>CN reaction at the G3 level.

barrier heights for the H + HCN reaction (reactions 34–39) have an AAD of only  $\sim 0.7$  kcal/mol. Although the test set in Table 2 is not meant to be comprehensive, it does show that the G3 theory can perform well for barrier height within “chemical accuracy” ( $\pm 2$  kcal/mol).

**III.2 Reaction Mechanism.** As shown in Figures 1 and 2, five kinds of reaction pathways in the H + CH<sub>3</sub>CN reaction were revealed. They are: direct hydrogen abstraction, C-addition/elimination, N-addition/elimination, H-migration, and H-to-CN substitution. We now consider them individually.

*A. Direct Hydrogen Abstraction.* The atomic hydrogen can abstract one of hydrogen atoms of the methyl group of the CH<sub>3</sub>CN molecule, forming H<sub>2</sub> and CH<sub>2</sub>CN. Transition state TS1 involved has C<sub>s</sub> symmetry and <sup>2</sup>A' state. The reacting H $\cdots$ H $\cdots$ C structure is nearly collinear with an angle of  $\sim 177^\circ$ . The breaking CH bond is elongated by  $\sim 0.2$  Å. The forming HH bond is 0.983 Å, which is 0.24 Å longer than the equilibrium distance of the free H<sub>2</sub> molecule. In view of these structural characteristics, TS1 is more reactant-like and thus an early barrier, as could be anticipated from the reaction exothermicity (by 7.8 kcal/mol at 0 K). Note that TS1 involves a large imaginary frequency (1427 cm<sup>-1</sup>), which is an indication of a narrow barrier and a significant tunneling effect. The corresponding barrier height is 12.0 kcal/mol.

*B. C-Addition/Elimination.* The H atom can add to the C atom of the CN group of CH<sub>3</sub>CN via transition state TS2 with the formation of CH<sub>3</sub>CHN radical. The forming CH bond is relatively long,  $\sim 1.86$  Å, which is  $\sim 0.76$  Å longer than that in the CH<sub>3</sub>CHN adduct. Evidently, TS2 is a rather early barrier, in accordance with the reaction exothermicity of 19.2 kcal/mol. Both TS2 and CH<sub>3</sub>CHN are of C<sub>s</sub> symmetry. Compared with the geometrical parameters of the reactant CH<sub>3</sub>CN, the CN bond in CH<sub>3</sub>CHN turns out to be of double character and its distance

increases by  $\sim 0.1$  Å. The CC single bond in CH<sub>3</sub>CHN is also slightly stretched. The barrier height is calculated to be 7.6 kcal/mol, 4.4 kcal/mol lower than that for the H-abstraction path.

With the internal energy of 19.2 kcal/mol, the adduct CH<sub>3</sub>CHN dissociates into CH<sub>3</sub> + HCN via transition state TS3. This is a CC bond scission process. The breaking CC bond in TS3 is elongated by up to 0.74 Å. The CN bond is shortened and the angle of HCN increases to 155.1°, tending to form the HCN product molecule. Meanwhile, the CH<sub>3</sub> group appears to be very similar to the final methyl free radical. This bond cleavage path is endothermic by 15.8 kcal/mol despite the overall exothermicity of 3.4 kcal/mol. The barrier height is 25.7 kcal/mol with respect to CH<sub>3</sub>CHN. Note that the energy of TS3 is 6.5 kcal/mol higher than that of the H + CH<sub>3</sub>CN reactants.

*C. N-Addition/Elimination.* Besides the C site, the terminal N site of the CH<sub>3</sub>CN molecule can be attacked by the H atom. However, this addition reaction occurs stereospecifically, that is, only *cis*-CH<sub>3</sub>CNH can be created. The corresponding transition state is TS4. The same reaction option has been found in the analogous H + HCN reaction.<sup>75–81</sup> As indicated by the long NH bond distance (1.62 Å), TS4 is a rather early barrier, in line with the reaction exothermicity (by 8.7 kcal/mol). The addition of H to N undergoes with the HNC orientation angle of 119.0°, and the CCN structure deviates somewhat from linearity. TS4 lies 9.6 kcal/mol above the reactants. This barrier is about 2 kcal/mol higher than that for the C-addition path.

The *trans* conformation of CH<sub>3</sub>CNH was also located, as shown in Figure 1. Except the HNCC dihedral angle, the geometries of the *trans* and *cis* conformers are nearly identical. Thermodynamically, the *trans*-CH<sub>3</sub>CNH is about 4.5 kcal/mol more stable than the *cis*-CH<sub>3</sub>CNH. However, the *cis*  $\rightarrow$  *trans* isomerization is rather difficult to occur because a high barrier (TS5) of 11.7 kcal/mol has to be surmounted along the reaction

TABLE 2: Barrier Heights (in kcal/mol) Calculated at the G3 Level<sup>a</sup>

| no. | reactions   | G3                       | previous work             | ref       |
|-----|---|--------------------------|---------------------------|-----------|
| 1   | H + H <sub>2</sub> → H <sub>2</sub> + H ( <sup>2</sup> Σ)                               | 10.2                     | 9.5                       | 17        |
| 2   | H + C <sub>2</sub> H <sub>2</sub> → H <sub>2</sub> + C <sub>2</sub> H ( <sup>2</sup> Σ) | 32.9                     | 33.0; 35.0                | 18        |
| 3   | O + NH → OH + N ( <sup>3</sup> Π)   | 12.8                     | 11.7                      | 19        |
| 4   | O + NH → OH + N ( <sup>3</sup> Π)   | 3.1                      | 5.5                       | 19        |
| 5   | O + H <sub>2</sub> → OH + H ( <sup>3</sup> Π)   | 13.0                     | 12.7; 12.5                | 20        |
| 6   | O + HCl → OH + Cl ( <sup>3</sup> A'')   | 10.1                     | 8.5                       | 21        |
| 7   | F + H <sub>2</sub> → HF + H ( <sup>2</sup> Σ)   | 0.7                      | 1.4 ± 0.4; 1.93; 2.1; 2.2 | 22        |
| 8   | Cl + H <sub>2</sub> → HCl + H ( <sup>2</sup> Σ)   | 8.7                      | 8.45; 9.6; 6.8            | 23        |
| 9   | OH + H <sub>2</sub> → H <sub>2</sub> O + H ( <sup>2</sup> A')                           | 6.6                      | 6.0; 5.7; 5.6             | 22(d), 24 |
| 10  | CH <sub>3</sub> + H <sub>2</sub> → CH <sub>4</sub> + H                                  | 12.9                     | 11.8; 12.6; 15.9; 13.5    | 22(d), 25 |
| 11  | NH <sub>2</sub> + H <sub>2</sub> → NH <sub>3</sub> + H ( <sup>2</sup> A')               | 10.9                     | 9.5; 10.8                 | 22(d)     |
| 12  | Cl + CH <sub>4</sub> → HCl + CH <sub>3</sub>  | 8.1                      | 7.9                       | 26        |
| 13  | OH + CH <sub>4</sub> → H <sub>2</sub> O + CH <sub>3</sub> ( <sup>2</sup> A')            | 7.4                      | 7.9; 6.6                  | 27        |
| 14  | O + CH <sub>4</sub> → OH + CH <sub>3</sub> ( <sup>3</sup> A'')                          | 13.7                     | 14.2; 14.0; 13.3; 13.6    | 28        |
| 15  | O + NH <sub>2</sub> → H–ONH   | -17.3                    | -15.4                     | 29        |
| 16  | O + NH <sub>2</sub> → H–N(H)O   | -23.8                    | -20.4                     | 29        |
| 17  | H + N <sub>2</sub> → HN <sub>2</sub> ( <sup>2</sup> A')                                 | 13.5                     | 15.2                      | 30        |
| 18  | H + NO → HNO ( <sup>3</sup> A'')  | 1.5                      | 4.1                       | 31        |
| 19  | N + O <sub>2</sub> → NOO ( <sup>2</sup> A')   | 6.1                      | 6.6; 6.2                  | 32(a)     |
| 20  | H + O <sub>2</sub> → HO <sub>2</sub> ( <sup>2</sup> A'')                                | 3.4                      | 3.4; 1.8; 9.2             | 32        |
| 21  | H + C <sub>2</sub> H <sub>2</sub> → C <sub>2</sub> H <sub>3</sub> ( <sup>2</sup> A')    | 2.9                      | 2.3                       | 33        |
| 22  | NH + NO → H–NNO ( <sup>2</sup> A')  | -23.2                    | -21.7                     | 34        |
| 23  | NH + NO → NN–OH ( <sup>2</sup> A')  | -14.0                    | -16.7                     | 34        |
| 24  | H + CO <sub>2</sub> → <i>cis</i> -HOCO ( <sup>2</sup> A')                               | 24.0                     | 25.4                      | 35        |
| 25  | H + CO <sub>2</sub> → HCO <sub>2</sub>  | 12.7                     | 11.3                      | 35        |
| 26  | NH <sub>2</sub> + NO → N <sub>2</sub> + H <sub>2</sub> O ( <sup>1</sup> A')             | -25.4                    | -21.9; -25.2              | 36        |
| 27  | CH <sub>3</sub> O → H + CH <sub>2</sub> O ( <sup>2</sup> A')                            | 23.5                     | 25.6                      | 37        |
| 28  | CH <sub>3</sub> OH → H <sub>2</sub> + CH <sub>2</sub> O ( <sup>1</sup> A')              | 91.4                     | 91.9                      | 38        |
| 29  | CH <sub>3</sub> O → CH <sub>2</sub> OH  | 30.2                     | 29.7                      | 39        |
| 30  | <i>trans</i> -HCOOH → <i>cis</i> -HCOOH   | 11.3                     | 10.9                      | 40        |
| 31  | CH <sub>3</sub> CN → CH <sub>3</sub> NC   | 63.5                     | 62.1                      | 3, 41     |
| 32  | HCN → HNC   | 46.4                     | 47.5; 45.2                | 3, 42     |
| 33  | C <sub>2</sub> H <sub>3</sub> → CH <sub>3</sub> C                                       | 54.0                     | 54.8~56.8                 | 43        |
| 34  | H + HCN → H <sub>2</sub> + CN ( <sup>2</sup> Σ)   | 30.6                     | 28.7; 30.5                | 44        |
| 35  | H <sub>2</sub> + CN → H + HCN ( <sup>2</sup> Σ)   | 5.0                      | 4.8; 6.2; 4.5; 5.3 ± 0.6  | 44        |
| 36  | H + HCN → CH <sub>2</sub> N ( <sup>2</sup> A')  | 8.0                      | 8.7; 10.7                 | 44        |
| 37  | H + HCN → <i>cis</i> -HCNH ( <sup>2</sup> A')   | 11.9                     | 12.1; 16.6                | 44        |
| 38  | H + HCN → <i>trans</i> -HCNH ( <sup>2</sup> A')   | 22.6                     | 21.8; 33.1                | 44        |
| 39  | <i>cis</i> -HCNH → <i>trans</i> -HCNH ( <sup>2</sup> A')                                | 10.6                     | 10.2; 10.3                | 44        |
|     | max ± deviation   | +3.5; -2.7               |                           |           |
|     | avg absolute deviation  | <b>1.12</b> <sup>b</sup> |                           |           |

<sup>a</sup> The UMP2(full)/6-31G(d) optimized geometries were employed. The values for reactions 1–25 correspond to the classical barrier heights, i.e., without ZPE corrections. The values for reactions 26–39 correspond to the barrier heights with the ZPE corrections (scaled by 0.93) at the UMP2(full)/6-31G(d) level. <sup>b</sup> The first values (the best values) in the fourth column were employed to calculate the average absolute deviation between the present G3 results and previous work.

path. Note that TS5 even lies 3.0 kcal/mol above the H + CH<sub>3</sub>CN reactants. It implies that the distinct *cis* and *trans* CH<sub>3</sub>CNH isomers cannot interchange rapidly in the H + CH<sub>3</sub>CN reaction. The transition state TS5 retains C<sub>s</sub> symmetry. The isomerization process occurs apparently through the in-the-plane anticlockwise rotational motion of the NH bond. The HNC structure in TS5 is very close to linearity.

Similar to the CH<sub>3</sub>CHN intermediate, both *cis* and *trans* CH<sub>3</sub>CNH can show CC bond scission via transition states TS6 and TS7, respectively, forming the same products, CH<sub>3</sub> + HNC. Except the HNCC dihedral angle, the structural parameters of TS6 and TS7 are very close. The breaking CC bond is elongated by ~0.85 Å. Thus, the two barriers are rather late, as indicated by the high endothermicity of the two reaction pathways. The overall production of CH<sub>3</sub> and HNC is endothermic by about 11.1 kcal/mol. The individual barrier heights are 28.1 and 33.1 kcal/mol, respectively.

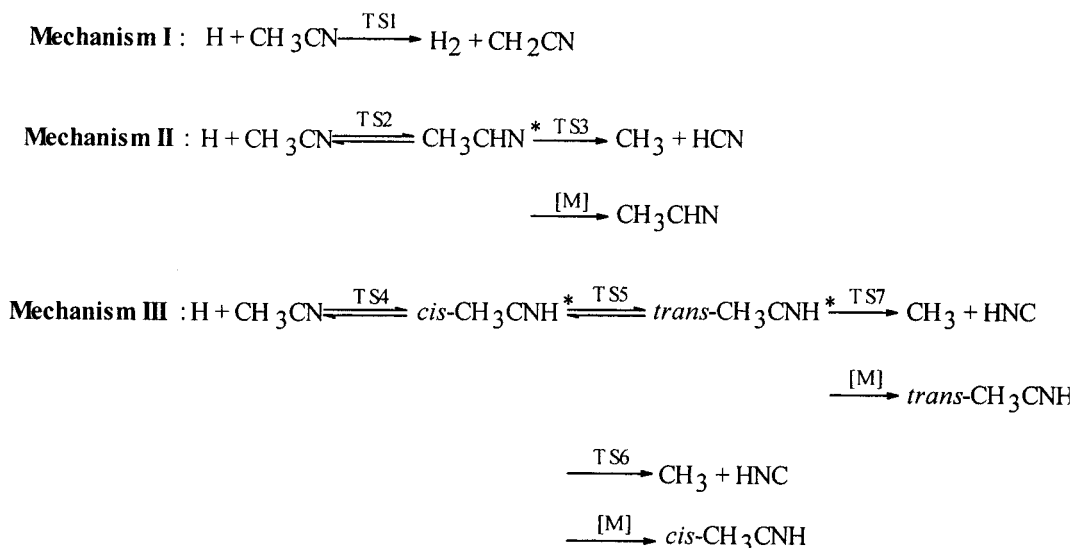
**D. H-Migration.** We also examined five possible hydrogen migration pathways along the CCN skeleton. The first reaction is 1,2-H shift from the C atom to the terminal N atom in the CH<sub>3</sub>CHN adduct, leading to the *trans*-CH<sub>3</sub>CNH radical via TS8. The methyl group acts as a spectator. The migrating hydrogen atom departs from the C and N atoms in the same distance,

~1.25 Å. The CCN bond angle in TS8 increases by about 12° in comparison with that in the CH<sub>3</sub>CHN radical. The barrier height is 42.5 kcal/mol.

The second reaction also starts from the CH<sub>3</sub>CHN radical. One of hydrogen atoms of the methyl group is shifted to the terminal N atom, forming the CH<sub>2</sub>CHNH radical. The transition state TS9 involved appears to be a four-center structure, and the two unreacting CH bonds of the methyl group are reflected by the HCCN plane. The breaking CH and the forming HN bonds are 1.46 and 1.32 Å, respectively. The CCN bond angle in TS9 decreases by up to 23° with respect to that one for the CH<sub>3</sub>CHN adduct. This reaction path is slightly endothermic (3.4 kcal/mol). The corresponding barrier height is 46.2 kcal/mol. It should be noted that TS9 has a <sup>2</sup>A' electronic state. In the IRC calculation, if this symmetry is conserved, a saddle point, which corresponds to the internal rotation of the CH<sub>2</sub> group around the CC bond of the CH<sub>2</sub>CHNH radical, will arrive. While the symmetry constraint is released, the planar CH<sub>2</sub>CHNH of <sup>2</sup>A'' ground electronic state is reached exactly in the product direction.

The CH<sub>2</sub>CHNH radical can be produced through another path, that is, the third H-migration reaction starting from the *cis*-CH<sub>3</sub>CNH radical. One of hydrogen atoms of the methyl group

## SCHEME 1

the H + CH<sub>3</sub>CN reaction:

shifts onto the neighbor C atom via three-center transition state TS10. The symmetry of the system breaks during the isomerization. As shown in Figure 1, the migrating H atom is out of the CCN plane by about 120°. The breaking CH bond and the forming HC bonds are 1.39 and 1.30 Å, respectively. The energy barrier is relatively high, 48.6 kcal/mol, even though the reaction is somewhat exothermic by 7.1 kcal/mol.

TS11 is the transition state for the fourth H-migration path: *trans*-CH<sub>3</sub>CNH → CH<sub>2</sub>CNH<sub>2</sub>. TS11 does keep C<sub>s</sub> symmetry, but the product CH<sub>2</sub>CNH<sub>2</sub> has no symmetry. Although this system breakdown at some points along the reaction coordinate might cause splitting of the path or double path degeneracy on going from the product to TS11, the IRC calculations confirm that only *trans* CH<sub>3</sub>CNH conformer is allied with the CH<sub>2</sub>CNH<sub>2</sub> radical. No transition state other than TS11 could be located. TS11 shows a 1,3-H shift option. The breaking CH bond is ~1.6 Å, which is elongated by about 0.5 Å. The forming HN bond is ~1.31 Å. The CCN bond angle in TS11 is about 17° and 21° smaller than those in CH<sub>3</sub>CNH and CH<sub>2</sub>CNH<sub>2</sub>, respectively. Meanwhile, the CC bond is shortened and the CN bond is stretched because the former becomes double bond and the latter turns out to be single bond in the CH<sub>2</sub>CNH<sub>2</sub> radical. The energy barrier for this H-shift pathway is very high, 71.0 kcal/mol relative to *trans*-CH<sub>3</sub>CNH. Additionally, the overall reaction H + CH<sub>3</sub>CN → CH<sub>2</sub>CNH<sub>2</sub> is nearly thermoneutral.

The last H-migration reaction is CH<sub>2</sub>CHNH → CH<sub>2</sub>CNH<sub>2</sub> via the 1,2-H shift transition state TS12. The bridging H atom is away from the migrating origin and terminus by 1.29 and 1.27 Å, respectively. The CCN bond angle increases from 126.6° to 141.9°. The CC bond is shortened and the CN bond is elongated in TS12. This reaction path involves a barrier of as high as 59.4 kcal/mol.

As shown in Figure 2, all of the barriers for these five H-migration pathways lie well above the reactants. Thus these channels are not important to the overall reaction rate. For completeness, we also examined two reaction pathways leading to the highly endothermic products H + CH<sub>2</sub>CNH. The first process is the CH bond scission of the CH<sub>2</sub>CHNH radical via transition state TS13. The two CH bonds of the methylene group first rotate around the CC bond until they become reflected by the HNCC mirror plane. Subsequently, the CH bond breaking

occurs, as indicated by the elongated distance of 1.88 Å. The second path is kicking off a hydrogen atom from the NH<sub>2</sub> group of the CH<sub>2</sub>CNH<sub>2</sub> radical via TS14. The breaking NH is stretched to 1.71 Å. In both TS13 and TS14, the CCN bond angles increase significantly, being very close to those in the product CH<sub>2</sub>CNH molecules. The barrier heights for these two reactions are 49.2 and 36.2 kcal/mol, respectively. It is interesting to note that the energies of TS13 and TS14 are very close, as shown by a difference of only 1.4 kcal/mol.

*E. H-to-CN Substitution.* The atomic hydrogen attacks to the methyl carbon of CH<sub>3</sub>CN, kicking off the CN group and forming the CH<sub>4</sub> molecule. The transition state for this substitution reaction, namely TS15 in Figure 1, exhibits simple structure of C<sub>3v</sub> symmetry where H attacks opposite to the departing CN radical. The forming HC bond is 1.358 Å, which is 0.27 Å longer than that in the CH<sub>4</sub> product. The breaking CC bond is stretched to 1.823 Å. The energy barrier for this reaction path is rather high, 44.7 kcal/mol. Moreover, the formation of CN and CH<sub>4</sub> is highly endothermic by 18.9 kcal/mol at 0 K. These characteristics are conceivable since the CC bond of CH<sub>3</sub>CN is much stronger than the CH bond of CH<sub>4</sub>. Therefore, it could be anticipated that this elementary substitution channel should play a negligible role in the title reaction. Jamieson et al.<sup>7</sup> proposed a CN propagated chain mechanism to account for their experimental observation that the amounts of both CH<sub>3</sub> and HCN produced were substantially higher than the flow rates of hydrogen atoms. However, in view of our theoretical calculation, the CN radical cannot be produced effectively in the H + CH<sub>3</sub>CN reaction at the temperature range studied (313~780 K). Therefore, the above chain mechanism might be unreliable. More extensive experiments are needed to clarify this issue.

It is worth noting that the potential energy surface relevant to the NH<sub>2</sub> + C<sub>2</sub>H<sub>2</sub> asymptote of the CH<sub>4</sub>CN system has been characterized by Moskaleva and Lin at the G2M level.<sup>15d</sup> Although the geometries were optimized at the B3LYP level only with the 6-311G(d,p) basis set, the computational results are satisfactory. Takayanagi et al.<sup>45</sup> also obtained a few species in Figure 1 in their study of the N(<sup>2</sup>D) + C<sub>2</sub>H<sub>4</sub> reaction at the PMP4/cc-pVTZ level with the MP2/cc-pVDZ geometries. However, the error in the relative energy for the H + CH<sub>3</sub>CN

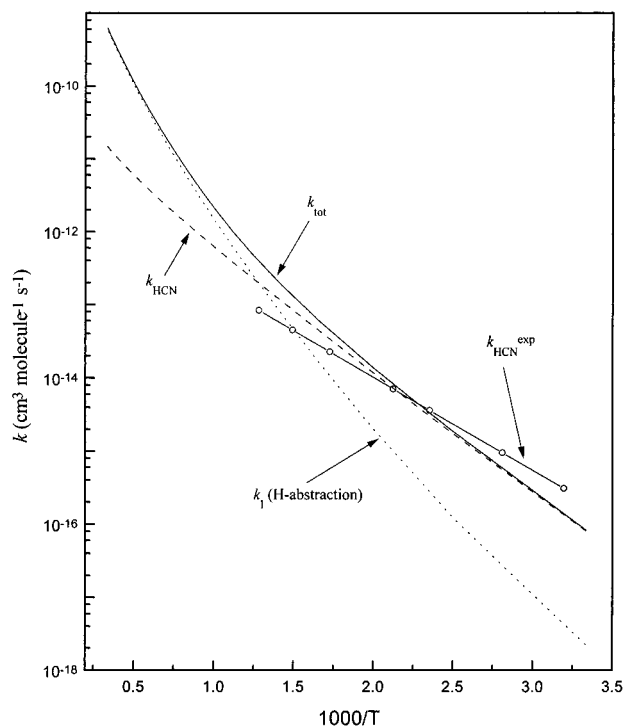


**Figure 3.** The calculated individual rate constants for the direct H-abstraction path ( $k_I$ ) and for the production of HCN ( $k_{\text{HCN}}$ ), and the total rate constant ( $k_{\text{tot}}$ ). The circles represent the experimental  $k_{\text{HCN}}$  values in the temperature range 313~780 K given in ref 7.

channel is as large as 8.4 kcal/mol, due to the unreliable MP wave functions. It implies that choosing the B3LYP method in our study should be apposite. Because of high reaction endothermicity, neither  $\text{NH}_2 + \text{C}_2\text{H}_2$  nor  $\text{N}(\text{D}) + \text{C}_2\text{H}_4$  asymptote is important to the title reaction.

**III.3. Rate Constants.** For simplicity, we choose the most important reaction channels, namely the following three mechanisms shown in Scheme 1, to calculate the rate constants of the  $\text{H} + \text{CH}_3\text{CN}$  reaction. The conventional transition state theory (CTST), including the unsymmetrical Eckart tunneling correction,<sup>46</sup> was employed to estimate the rate constants for mechanism I. For mechanisms II and III, the multichannel RRKM procedure, which has been detailed in the Note S1 of the Supporting Information, was used. It has been shown that this method is successful to access the kinetics of the complex-forming bimolecular reactions. The essential parameters, including moments of inertia and vibrational frequencies, have been listed in Table S1.

We first calculated the individual and total rate constants at the temperature range of 300~3000 K and at the pressure of 1 Torr of  $\text{H}_2$  in order to compare with the previous experimental results.<sup>7</sup> Under these conditions, only the formations of  $\text{H}_2 + \text{CH}_2\text{CN}$  and  $\text{CH}_3 + \text{HCN}$  in mechanisms I and II, respectively, have the observable rates, as shown in Figure 3. The rate constants for the other channels are always a few orders of magnitude lower and thus are negligible. It can be seen from Figure 3 that our calculated rate constants for the production of HCN,  $k_{\text{HCN}}$ , are in reasonable agreement with the experimental values at the temperatures 313~780 K within the factors of 0.4~2.3. At lower temperatures, the  $\text{H} + \text{CH}_3\text{CN}$  reaction is dominated by mechanism II. Thus, the major products are  $\text{CH}_3$  and HCN. With the elevation of temperature, mechanism I, i.e., the direct H-abstraction, becomes competitive, and it indeed dominates the reaction at temperatures above 1000 K. Thus, it can be expected that at flames the major products of

**TABLE 3: Individual and Total Rate Constants for the Reaction of H with  $\text{CH}_3\text{CN}$ , Fitted to the Three-Parameter Formula:  $k = A T^n e^{-E/T}$  over the Range of  $300 \leq T \leq 3000$  K**

| $k_i^a$                 | $A^b$  | $n$           | $E^c$         |
|-------------------------|--|---------------|---------------|
| $k_I$                   | $1.01 \times 10^{-19}$   | 3.01          | 4289          |
| $k_{\text{HCN}}$        | $7.36 \times 10^{-14}$ ( $3.16 \times 10^{-12}$ ) <sup>d</sup> | 0.80 (0.36)   | 3421 (4105)   |
| $k_{\text{II}}^\infty$  | $2.13 \times 10^{-14}$   | 0.99          | 3346          |
| $k_{\text{HNC}}$        | $4.68 \times 10^{-9}$ ( $5.22 \times 10^{-9}$ )                | -0.32 (-0.34) | 10083 (10105) |
| $k_{\text{III}}^\infty$ | $4.59 \times 10^{-13}$   | 0.65          | 4353          |
| $k_{\text{tot}}$        | $1.24 \times 10^{-22}$ ( $9.58 \times 10^{-23}$ )              | 3.77 (3.80)   | 2450 (2381)   |
| $k_{\text{tot}}^\infty$ | $2.49 \times 10^{-21}$   | 3.40          | 2649          |

<sup>a</sup>  $k_I$  stands for the rate constant for the mechanism I (direct H-abstraction);  $k_{\text{HCN}}$  is the rate constant of production of HCN in mechanism II (C-addition);  $k_{\text{HNC}}$  is the rate constant of production of HNC in mechanism III (N-addition);  $k_{\text{tot}}$  is the total rate constant.  $k_{\text{II}}^\infty$ ,  $k_{\text{III}}^\infty$ , and  $k_{\text{tot}}^\infty$  represent the high-pressure limit rate constants for mechanisms II, III, and overall reaction, respectively. <sup>b</sup> In  $\text{cm}^3 \text{ molecule}^{-1} \text{ s}^{-1}$ . <sup>c</sup> In K. <sup>d</sup> The values are given for 1 and 760 (in brackets) Torr of Ar, respectively.

the  $\text{H} + \text{CH}_3\text{CN}$  reaction might be hydrogen and cyanomethyl radical.

For practical use, we have calculated the individual and total rate constants at the pressures of 1 and 760 Torr of Ar, and at high-pressure limit. The results were fitted to an empirical three-parameter expression, i.e.,  $k = AT^n e^{-E/T}$ , in units of  $\text{cm}^3 \text{ molecule}^{-1} \text{ s}^{-1}$ . The best-fit parameters are listed in Table 3.

We prefer to discuss a few interesting findings using the data in Table 3. At  $T = 300$  K, the contribution of H-abstraction was found to be always negligible. From  $P = 1$  Torr to  $P = 760$  Torr, the rate constants for the formation of HCN ( $k_{\text{HCN}}$ ) decrease by about three times, and the branching ratios are reduced from ~100% to ~31%. It implies that  $k_{\text{HCN}}$  lies in the falloff region. At high-pressure limit, the mechanism II, which is effectively the stabilization of the  $\text{CH}_3\text{CHN}^*$  adduct, becomes dominant with a branching ratio of ~88% since the C-addition step involves the lowest energy barrier. The N-addition (mechanism III) is only a minor channel with a branching ratio of ~10%. When the temperature is elevated to 3000 K, the direct H-abstraction is apparently the dominant reaction path. The corresponding yield always exceeds 95%. At the pressures 1~760 Torr or at the high-pressure limit, the rate constants  $k_{\text{HCN}}$ ,  $k_{\text{II}}$ , and  $k_{\text{III}}$  are all negligible. Before the further experimental study appears, these state-of-the-art theoretical predictions might be useful as an at least qualitative estimate to the kinetics of the reaction of atomic hydrogen with acetonitrile.

#### IV. Conclusions

We report a theoretical study of the lowest potential energy surface for the  $\text{H} + \text{CH}_3\text{CN}$  reaction at the G3//B3LYP/6-311++G(2d,2p) level. As indicated by the calibration calculation, this PES is probably reliable within chemical accuracy. The  $\text{H} + \text{CH}_3\text{CN}$  reaction can start in four kinds of manners, i.e., direct hydrogen abstraction, additions to C and N sites, respectively, and H-to-CN substitution. At lower temperatures the C-addition path is the most favorable, and the major products are  $\text{CH}_3 + \text{HCN}$  at lower pressures. However, at higher temperatures, for instance, in flames, the H-abstraction channel, leading to  $\text{H}_2 + \text{CH}_2\text{CN}$ , is dominant.

**Supporting Information Available:** Table S1 presents the moments of inertia and vibrational frequencies of various species in the  $\text{H} + \text{CH}_3\text{CN}$  reaction at the B3LYP/6-311++G(2d,2p) level. Note S1 details the rate constant formula for mechanisms II and III deduced using the RRKM-TST model. This material is available free of charge via the Internet at <http://pubs.acs.org>.

## References and Notes

- (1) Hamm, S.; Warneck, P. *J. Geophys. Res.* **1990**, *95*, 20593.
- (2) Lide, D. R. *CRC Handbook of Chemistry and Physics*, 74th ed.; CRC: Boca Raton, FL, 1993.
- (3) Jursic, B. S. *Chem. Phys. Lett.* **1996**, *256*, 213.
- (4) Tyndall, G. S.; Orlando, J. J.; Wallington, T. J.; Sehested, J.; Nielsen, O. *J. Phys. Chem.* **1996**, *100*, 660, and references therein.
- (5) Budge, S.; Roscoe, J. M. *Can. J. Chem.* **1995**, *73*, 666.
- (6) Hynes, A. J.; Wine, P. H. *J. Phys. Chem.* **1991**, *95*, 1232.
- (7) Jamieson, J. W. S.; Brown, G. R.; Tanner, J. S. *Can. J. Chem.* **1970**, *48*, 3619.
- (8) (a) Baker, J.; Scheiner, A. C.; Andzelm, J. J. *Chem. Phys. Lett.* **1993**, *216*, 380. (b) Baker, J.; Muir, M.; Andzelm, J. J. *Chem. Phys.* **1995**, *102*, 2065.
- (9) Becke, A. D. *J. Chem. Phys.* **1993**, *98*, 5648.
- (10) Lee, C.; Yang, W.; Parr, R. G. *Phys. Rev.* **1988**, *B37*, 785.
- (11) (a) Fukui, K.; Kato, S.; Fujimoto, H. *J. Am. Chem. Soc.* **1975**, *97*, 1. (b) Ishida, K.; Morokuma, K.; Komornicki, A. *J. Chem. Phys.* **1977**, *66*, 2153. (c) Gonzalez, Z.; Schlegel, H. B. *J. Phys. Chem.* **1989**, *90*, 2154.
- (12) Curtiss, L. A.; Raghavachari, K.; Redfern, P. C.; Rassolov, V.; Pople, J. A. *J. Chem. Phys.* **1998**, *109*, 7764.
- (13) Frisch, M. J.; Trucks, G. W.; Schlegel, H. B.; Gill, P. W. M.; Johnson, B. G.; Robb, M. A.; Cheeseman, J. R.; Keith, T. A.; Petersson, G. A.; Montgomery, J. A.; Raghavachari, K.; Allaham, M. A.; Zakrzewski, V. G.; Ortiz, J. V.; Foresman, J. B.; Cioslowski, J.; Stefanov, B. B.; Nanayakkara, A.; Challacombe, M.; Peng, C. Y.; Ayala, P. Y.; Chen, W.; Wong, M. W.; Andres, J. L.; Replogle, E. S.; Gomperts, R.; Martin, R. L.; Fox, D. J.; Binkley, J. S.; Defrees, D. J.; Baker, J.; Stewart, J. P.; Head-Gordon, M.; Gonzales, C.; Pople, J. A. *Gaussian 94*; Gaussian Inc.: Pittsburgh, PA, **1995**.
- (14) Afeefy, H. Y.; Liebman, J. F.; Stein, S. E. In *NIST Chemistry WebBook*, NIST Standard Reference Database; <http://webbook.nist.gov>.
- (15) (a) Wang, B.; Hou, H.; Gu, Y. *J. Chem. Phys.* **2000**, *112*, 8458. (b) Davis, S. G.; Law, C. K.; Wang, H. *J. Phys. Chem. A* **1999**, *103*, 9241. (c) Vereecken, L.; Pierloot, K.; Peeters, J. *J. Chem. Phys.* **1998**, *108*, 1068. (d) Moskaleva, L. V.; Lin, M. C. *J. Phys. Chem. A* **1998**, *102*, 4687.
- (16) (a) Chase, M. W., Jr.; Davies, C. A.; Downey, J. R., Jr.; Frurip, D. J.; McDonald, R. A.; Syverud, A. N. *J. Phys. Chem. Ref. Data* **1985**, *14*, Suppl. No. 1. (b) Atkinson, R.; Baulch, D. L.; Cox, R. A.; Hampson, R. F.; Kerr, J. A.; Troe, J. *J. Phys. Chem. Ref. Data* **1992**, *21*, 1125.
- (17) (a) Boothroyd, A. J.; Kcogh, W. J.; Martin, P. G.; Peterson, M. R. *J. Chem. Phys.* **1991**, *95*, 4343. (b) Truhlar, D. G.; Horowitz, C. J. *J. Chem. Phys.* **1978**, *68*, 2466. (c) Siegbahn, P.; Liu, B. *ibid* **1978**, *68*, 2457.
- (18) (a) Wang, D.; Bowman, J. M. *J. Chem. Phys.* **1994**, *101*, 8646. (b) Harding, L. B.; Schatz, G. C.; Chiles, R. A. *J. Chem. Phys.* **1982**, *76*, 5172.
- (19) Walch, S. P. *J. Chem. Phys.* **1990**, *93*, 8036.
- (20) (a) Schatz, G. C. *J. Chem. Phys.* **1985**, *83*, 5677. (b) Walch, S. P.; Dunning, T. H., Jr.; Raffanetti, R. C.; Bobrowicz, F. W. *J. Chem. Phys.* **1980**, *72*, 406. (c) Walch, S. P. *J. Phys. Chem.* **1987**, *86*, 5670.
- (21) Koizumi, H.; Schatz, G. C.; Gordon, M. S. *J. Chem. Phys.* **1991**, *95*, 6421.
- (22) (a) Bauschlicher, C. W.; Walch, S. P.; Langhoff, S. R.; Taylor, P. R.; Jaffe, R. L. *J. Chem. Phys.* **1988**, *88*, 1743. (b) Knowles, P. J.; Stark, K.; Werner, H. J. *Chem. Phys. Lett.* **1991**, *185*, 555. (c) Scuseria, S. S. *J. Chem. Phys.* **1991**, *95*, 7426. (d) Kraka, S. S.; Gauss, J.; Cremer, D. *J. Chem. Phys.* **1993**, *99*, 5306.
- (23) (a) Werner, H.-J., private communication. (b) Bian, W.; Werner, H.-J. *J. Chem. Phys.* **2000**, *112*, 220. (c) Bian, W.; Werner, H.-J. *Science* **1999**, *286*, 1713. (d) Bian, W.; Werner, H.-J. *Chem. Phys. Lett.* **1999**, *313*, 647. (e) Harding, L. B., private communication. At the CAS+1+2 (4s, 3p, 2d, 1f/3s, 2p, 1d) + Davidson correction. (f) Kumaran, S. S.; Lim, K. P.; Michael, J. V. *J. Chem. Phys.* **1994**, *101*, 9487.
- (24) (a) Walch, S. P.; Dunning, T. H., Jr. *J. Chem. Phys.* **1980**, *72*, 1303. (b) Schatz, G. C.; Elgersma, H. *Chem. Phys. Lett.* **1980**, *73*, 21. (c) Dunning, T. H., Jr.; Harding, L. B.; Kraka, E. *Supercomputer Algorithms for Reactivity, Dynamics and Kinetics of Small Molecules*; Lagana, A., Ed.; Kluwer Academic: Dordrecht, Holland, 1989; p57. (d) Schlegel, H. B.; Sosa, C. *Chem. Phys. Lett.* **1988**, *145*, 329.
- (25) (a) Walch, S. P. *J. Chem. Phys.* **1980**, *72*, 4932. (b) Schatz, G. C.; Walch, S. P.; Wagner, A. F. *J. Chem. Phys.* **1980**, *73*, 4536. (c) Schatz, G. C.; Wagner, A. F.; Dunning, T. H., Jr. *J. Phys. Chem.* **1984**, *88*, 221. (d) Steckler, R.; Dykema, K. J.; Brown, F. B.; Hancock, G. C.; Truhlar, D. G.; Valencich, T. *J. Chem. Phys.* **1987**, *87*, 7024.
- (26) Truong, T. N.; Truhlar, D. G.; Baldrige, K. K.; Gordon, M. S.; Steckler, R. *J. Chem. Phys.* **1989**, *90*, 7137.
- (27) (a) Truong, T. N.; Truhlar, D. G. *J. Chem. Phys.* **1990**, *93*, 1761. (b) Dobbs, K. D.; Dixon, D. A.; Komornicki, A. *J. Chem. Phys.* **1993**, *98*, 8852.
- (28) (a) Robert-Neto, O.; Machado, F. B. C.; Truhlar, D. G. *J. Chem. Phys.* **1999**, *111*, 10046. (b) Corchado, J. C.; Espinosa-Garcia, J.; Robert-Neto, O.; Chuang, Y.; Truhlar, D. G. *J. Phys. Chem. A* **1998**, *102*, 4899. (c) Gonzalez, M.; Hernandez, J.; Millan, J.; Sayos, R. *J. Chem. Phys.* **1999**, *110*, 7326. (d) Walch, S. P.; Dunning, T. H., Jr. *J. Chem. Phys.* **1980**, *72*, 3221.
- (29) Walch, S. P. *J. Chem. Phys.* **1993**, *99*, 3804.
- (30) (a) Walch, S. P.; Duchovic, R. J.; Rohlfing, C. M. *J. Chem. Phys.* **1989**, *90*, 3230. (b) Walch, S. P. *J. Chem. Phys.* **1990**, *93*, 2384.
- (31) Walch, S. P.; Rohlfing, C. M. *J. Chem. Phys.* **1989**, *91*, 2939.
- (32) (a) Durant, J. L., Jr.; Rohlfing, C. M. *J. Chem. Phys.* **1993**, *98*, 8031. (b) Mebel, A. M.; Morokuma, K.; Lin, M. C. *J. Chem. Phys.* **1995**, *103*, 7414. (c) Walch, S. P.; Duchovic, R. J. *J. Chem. Phys.* **1991**, *94*, 7068.
- (33) Harding, L. B.; Wagner, A. F.; Bowman, J. M.; Schatz, G. C.; Christoffel, K. *J. Phys. Chem.* **1982**, *86*, 4312.
- (34) Walch, S. P. *J. Chem. Phys.* **1993**, *98*, 1170.
- (35) (a) Schatz, G. C.; Fitzcharles, M. S.; Harding, L. B. *Faraday Discuss. Chem. Soc.* **1987**, *84*, 359. (b) Kudla, K.; Schatz, G. C.; Wagner, A. F. *J. Chem. Phys.* **1991**, *95*, 1635. (c) Schatz, G. C. *Rev. Mod. Phys.* **1989**, *61*, 669.
- (36) (a) Walch, S. P. *J. Chem. Phys.* **1993**, *99*, 5295. (b) Melius, C. F.; Binkley, J. S. *20th Symposium (International) on Combustion*; The Combustion Institute: Pittsburgh, PA, 1984.
- (37) Page, M.; Lin, M. C.; He, Y.; Choudhury, T. K. *J. Phys. Chem.* **1989**, *93*, 4404.
- (38) Walch, S. P. *J. Chem. Phys.* **1993**, *98*, 3163.
- (39) Batt, L.; Burrows, J. P.; Robinson, G. N. *Chem. Phys. Lett.* **1981**, *78*, 467.
- (40) (a) Hocking, W. H. *Naturforsch. Z. Teil A* **1976**, *31*, 1113. (b) Bjarnov, E.; Hocking, W. H. *Naturforsch. Z. Teil A* **1978**, *33*, 610.
- (41) Schneider, F. W.; Rabinovitch, B. S. *J. Am. Chem. Soc.* **1962**, *84*, 4115.
- (42) (a) Nguyen, M. T.; Groarke, P. G.; Malone, S.; Hegarty, A. F. *J. Chem. Soc., Perkin Trans. 2*, **1994**, 807. (b) Lee, T. J.; Rendell, A. P. *Chem. Phys. Lett.* **1991**, *177*, 491. (c) Bentley, J. A.; Bowman, J. M.; Gazdy, B.; Lee, T. J.; Dateo, C. E. *Chem. Phys. Lett.* **1992**, *198*, 563. (d) Bowman, J. M.; Gazdy, B.; Bentley, J. A.; Lee, T. J.; Dateo, C. E. *J. Chem. Phys.* **1993**, *99*, 308. (e) Thomas, J. R.; DeLeeuw, B. J.; Vacek, G.; Crawford, T. D.; Yamaguchi, Y.; Schaefer, H. F., III. *J. Chem. Phys.* **1993**, *99*, 403.
- (43) Nielsen, I. M. B.; Janssen, C. L. Burton, N. A.; Schaefer, H. F., III. *J. Phys. Chem.* **1992**, *96*, 2490.
- (44) (a) Sumathi, R.; Nguyen, M. T. *J. Phys. Chem. A* **1998**, *102*, 8013. (b) Bair, R. A.; Dunning, T. H., Jr. *J. Chem. Phys.* **1985**, *82*, 2280. (c) ter Horst, M. A.; Schatz, G. C.; Harding, L. B. *J. Chem. Phys.* **1996**, *105*, 558. (d) Brooks, A. N.; Clary, D. C. *J. Chem. Phys.* **1990**, *92*, 4178. (e) Clary, D. C. *J. Phys. Chem.* **1995**, *99*, 13664. (f) Wagner, A. F.; Bair, R. A. *Int. J. Chem. Kinet.* **1986**, *18*, 473. (g) Schacke, H.; Wagner, H. Gg.; Wolfrum, J. *Ber. Bunsen-Ges. Phys. Chem.* **1977**, *81*, 670.
- (45) Takayanagi, T.; Kurosaki, Y.; Sato, K.; Tsunashima, S. *J. Phys. Chem. A* **1998**, *102*, 10391.
- (46) Johnston, H. S.; Heicklen, J. *J. Phys. Chem.* **1962**, *66*, 532.